J Mater Sci (2016) 51:3592–3599
DOI 10.1007/s10853-015-9679-4

Effects of Zn-doping on structure and electrical properties of p-type conductive $CuCr_{1-x}Zn_xO_2$ delafossite oxide

Ya-Hui Chuai[1] · Xin Wang[1] · Hong-Zhi Shen[1] · Ya-Dan Li[2] · Chuan-Tao Zheng[1,3] · Yi-Ding Wang[1]

Received: 15 October 2015 / Accepted: 15 December 2015 / Published online: 28 December 2015
© Springer Science+Business Media New York 2015

Abstract Delafossite-type $CuCr_{1-x}Zn_xO_2$ ($x = 0$, 0.03, 0.05, 0.07, 0.1) conductive oxides were synthesized by sol–gel method, and the effects of Zn-doping on morphology, structure, and electrical properties of the $CuCr_{1-x}Zn_xO_2$ oxides were investigated. Based on X-ray diffraction (XRD) and Raman spectrum, the crystalline quality of the oxides is improved by the suitable substitution of Cr by Zn. The X-ray photoelectron spectroscopy (XPS) spectra reveal the chemical state of Zn is +2. The Hall and Seebeck coefficients of the pellet samples display a positive sign, indicating p-type conductive characteristics of the obtained oxides. The temperature-dependent resistivity of the oxides is proven to be consistent with small polaron hopping. For the three oxide samples with $x = 0$, 0.05, and 0.1, the activation energies for the polaron hopping between Zn^{2+} and Cr^{3+} sites are 54, 41.5, 32 meV, respectively, which is found to decrease with the increase of Zn content. The electrical conductivity can be remarkably improved by Zn-doping due to the small polaron hopping activation energy. These properties render this material promising as transparent electrode in optoelectronic industry.

✉ Chuan-Tao Zheng
zhengchuantao@jlu.edu.cn

✉ Yi-Ding Wang
ydwang@jlu.edu.cn

[1] State Key Laboratory on Integrated Optoelectronics, College of Electronic Science and Engineering, Jilin University, 2699 Qianjin Street, Changchun 130012, People's Republic of China

[2] College of Physics, Jilin University, 2699 Qianjin Street, Changchun 130012, People's Republic of China

[3] Department of Electrical and Computer Engineering, Rice University, 6100 Main Street, Houston, TX 77005, USA

Introduction

Transparent conductive oxides (TCOs) play an important role in transparent electrodes and photovoltaic industry. They are widely used in flat panel display, touch panel, solar cell, and light-emitting diode [1, 2], due to their functional combination of optical transparency and electrical conductivity in visible band. It is well known that most TCOs are n-type semiconductors, such as In_2O_3 [3], ZnO [4], and SnO_2 [5]. However, in most applications, such as light-emitting diode and functional window, both n-type and p-type transparent conductive materials are required. Therefore, p-type TCO has been a worldwide hot research issue. In 1997, Kawazoe et al. first found that copper aluminum oxide ($CuAlO_2$) was a kind of p-type TCO material with a direct energy gap of 3.5 eV and positive Seebeck coefficient, and they also showed that $CuAlO_2$ possesses an electrical conductivity in the level of 1 S/cm at room temperature [6]. The discovery of p-type TCO makes it possible for people to fabricate transparent oxide optoelectronic devices, such as transparent p–n junction diode and transistor using an appropriate combination of p-type and n-type TCO complementary techniques of Si-based electronics [7]. However, the conductivity of p-type TCO compounds is much lower than that of the more commonly used n-type TCOs, like Sn-doped In_2O_3. For the practical applications of p-type TCOs, the improvement of electrical property seems to be very exigent demanding and necessary, in order to achieve similar properties with n-type oxides [8].

At present, $CuXO_2$ (X = Al, Fe, Ga, Cr and In) has become an important kind of p-type TCOs, and both theoretical and experimental researches have been carried out to explore high-performance and low-cost delafossite-type TCOs. Using the first-principle calculation, Nakanishi et al.

revealed that $CuAlO_2$ has great potential to be p-type transparent superconductors [9]. With solid-state reaction method, Dong et al. synthesized $CuNdO_2$ delafossite, which is a p-type transparent conductive oxide with an optical bandgap of 3.14 eV [10]. In our previous work, using sol–gel method, we prepared $CuFe_{1-x}Sn_xO_2$ films on Al_2O_3 (001) substrates for growing orientations [11]. Delafossite compound belongs to the family of ternary oxide, whose general and chemical formulas are ABO_2 and $A^+B^{3+}O_2$, respectively. Compared with the delafossite compounds $CuXO_2$ (X = Al, Ga) [12], $CuCrO_2$ has drawn more attention owning to low synthesis temperature and good thermal stability. The structure of delafossite $CuCrO_2$ can be treated to be consisted of two alternative layers: a planar layer of Cu cation in a triangular pattern and a CrO_2 layer with Cr^{3+}-centered edge-sharing octahedra. Each Cu atom is linearly coordinated with two oxygen atoms to form an O–Cu–O dumbbell unit which is parallel to *c*-axis [13]. The crystal structure of $CuCrO_2$ can be described by a rhombohedral spatial group $R\bar{3}m$, and there are only four atoms (one Cu, one Cr, and two O atoms) in the primitive rhombohedral cell. In the close energy proximity with O 2p levels, the hybridization of Cu $3d^{10}$ energy levels increases the energy of the valence band maximum value, and also it delocalizes the hole state to form an intrinsic p-type semiconductor [14]. For $CuScO_2$ and $CuYO_2$ compounds, the intercalation of oxygen to form $CuMO_{2+x}$ phases will improve their conductivity [15]. However, because of small ionic radius of Cr (0.615 Å), the conductivity of $CuCrO_2$ cannot be easily improved by the intercalation of oxygen [16]. Therefore, the intrinsic resistance of $CuCrO_2$ films is too large to be suitable for practical application. Up to now, it is well known that the introduction of some metal ions into TCOs could effectively increase both carrier density and electrical conductivity. Though this type of carrier doping has been widely used in n-type semiconductors, only a few studies have reported successful p-type doping for oxide semiconductors [17–19].

In this article, in order to improve the conductivity of $CuCrO_2$ compound, we reported our effort to synthesis polycrystalline delafossite oxides of $CuCr_{1-x}Zn_xO_2$ ($x = 0$, 0.03, 0.05, 0.07, 0.1) by the general chemical solution process. We also investigated the effects of Zn^{2+}-doping on the structure and electrical properties of such compound. The rest of this paper is organized as follows. First in "Experiment and measurement" section, experimental details for the synthesis and measurement of the $CuCr_{1-x}Zn_xO_2$ oxides are described. Then in "Results and discussion" section, measurement results as well as related analysis and discussion are given, including field emission scanning electron microscope (FESEM) characterization, crystalline structure, X-ray photoelectron spectroscopy (XPS), optical property based on Fourier transform infrared spectrometer (FTIR), thermal and electrical properties. Finally, some conclusions are reached in "Conclusion" section.

Experiment and measurement

Preparation of $CuCr_{1-x}Zn_xO_2$ powder

Polycrystalline delafossite oxides $CuCr_{1-x}Zn_xO_2$ ($x = 0$, 0.03, 0.05, 0.07, 0.1) were prepared by sol–gel method. Analytically pure copper acetate [$Cu(AcO)_2{\cdot}H_2O$], chromium nitrate [$Cr(NO_3)_3{\cdot}9H_2O$], and zinc acetate [$Zn(AcO)_2{\cdot}2H_2O$] were used as starting materials. Specifically, copper acetate (1.9965 g, 0.01 mol) was dissolved in 30 mL anhydrous ethanol and stirred for about 30 min, yielding a blue transparent solution. After the solution gets stable and homogeneous, the required chromium nitrate hydrate and zinc acetate hydrate were added into the solution. The mass was counted by the mole ratio of Zn/Cr. The solution was stirred for more than 5 h at 45 °C in order to get a well-mixed precursor solution. The resulting solution was baked and fully grinded in an agate mortar and sintered in air at 1000 °C for 10 h.

Preparation of $CuCr_{1-x}Zn_xO_2$ pellets

The $CuCr_{1-x}Zn_xO_2$ powder was pressed into pellets with 15 mm diameter and 2.5 mm thickness under 21 Mpa using a powder tableting machine (769YP-40C). The resulting pellets were sintered in air at 1000 °C for another 24–48 h until the samples with pure phase were obtained. Furthermore, ohmic contact was formed on a pallet for Hall measurement. On four symmetric positions of the circle pellet, four electrodes were made with Indium. Following that, put the pallet into a short annealing furnace for half an hour to form ohmic contact finally.

Characterization and measurement

The morphology of $CuCr_{1-x}Zn_xO_2$ samples was observed by a JSM-7500F FESEM. Crystal structure was analyzed using the conventional X-ray diffractometer (XRD) technique with a Bruker D8 Advance X, Pert diffractometer (Cu Ka = 1.540 Å), and the scanning speed was 4°/min from 10° to 70°. Raman spectra were recorded at room temperature with the 514.5 nm line of an Ar^+ laser, excitation from a Spectra Physics krypton ion laser. XPS

(ESCALAB 250) was used to determine the chemical composition and valence of the elements. FTIR spectra for bonding information were investigated on the powder samples using an FTIR (Perkin-Elmer Spectrum GX FTIR/FT-Raman spectrometer) in the range of 400–4000 cm^{-1}. Thermogravimetry and differential thermal analysis (TG–DTA) of the precursor material was carried out with a SDT Q600 V20.9 model. Electrical properties were determined using a Hall-effect measurement system (ACCENT HL55OOPC) at room temperature and ULVAC-RIKO ZEM-2 thermoelectric property measurement system under a low-pressure helium atmosphere.

Results and discussion

FESEM analysis

The SEM observation in Fig. 1 reveals the morphologies of the sol–gel-derived delafossite-$CuCr_{1-x}Zn_xO_2$-polycrystalline post-annealed at 1000 °C in air for 24 h. As can be seen from Fig. 1f, the rhombohedral *R*-3 m $CuCr_{1-x}Zn_xO_2$ crystal appears to be hexagonal slices. It is also found that as Zn-doping ratio increases, the grain size is enlarged within a wide range of particle size distribution varying from 0.8 to 18 μm.

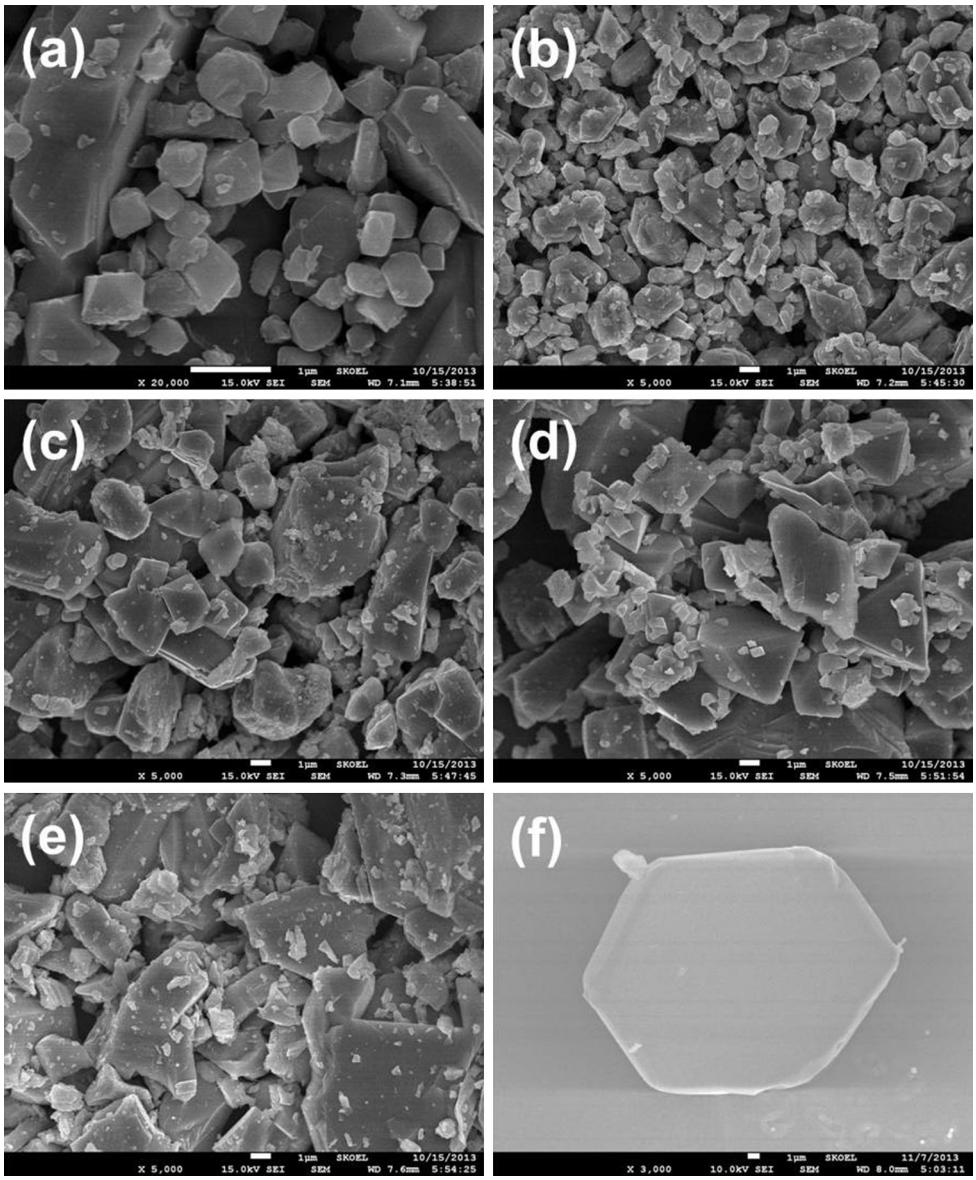

Fig. 1 FESEM images of the $CuCr_{1-x}Zn_xO_2$ samples. **a–e** are corresponding to the Zn-doping ratios of $x = 0$, 0.03, 0.05, 0.07, 0.1, respectively. **f** is the amplified $CuCr_{0.9}Zn_{0.1}O_2$ crystal grain

Structure characterization

Figure 2a shows the XRD patterns of the derived sol–gel $CuCr_{1-x}Zn_xO_2$ samples ($x = 0$, 0.03, 0.05, 0.07, and 0.1) post-annealed at 1000 °C in air. The XRD peaks of a $CuCrO_2$ sample will display the phase of delafossite structure (JCPDS file: 39-0247) and the impurity phase of CuO (ICSD Card File:01-089-5897). The obtained XRD patterns show all the peaks of $CuCrO_2$ sample and those of CuO, which confirms that the formed $CuCr_{1-x}Zn_xO_2$ possesses delafossite structure. The XRD peaks of the $CuCr_{1-x}Zn_xO_2$ solid solution shift toward lower angles with Zn-doping, as can be seen in the magnified XRD patterns of the (018) peak displayed in Fig. 2b. The lattice spacing parameters of the $CuCr_{1-x}Zn_xO_2$ samples ($x = 0$, 0.03, 0.05, 0.07, and 0.1) are exhibited in Table 1. The lattice parameters along a-axis and c-axis are 2.9762 and 17.1024 Å, respectively, which are in good agreement with $CuCrO_2$ (JCPDS No. 39-0247 $a = 2.976$ Å and $c = 17.102$ Å). Also, the two parameters rapidly increase as increasing the Zn content. This effect occurs due to the partial substitution of Zn^{2+} (0.74 Å) with large ionic radii into Cr^{3+} (0.615 Å) sites with small radii, leading to local lattice distortion [20].

Table 1 The lattice parameters of the $CuCr_{1-x}Zn_xO_2$ ($x = 0$, 0.03, 0.05, 0.07, 0.1) samples

Composition	a (Å)	c (Å)	Cell volume (Å^3)
$CuCrO_2$	2.9762 (3)	17.1024 (5)	131.181 (6)
$CuCr_{0.97}Zn_{0.03}O_2$	2.9801 (3)	17.0939 (2)	138.233 (7)
$CuCr_{0.95}Zn_{0.05}O_2$	2.9884 (2)	17.0897 (4)	141.361 (3)
$CuCr_{0.93}Zn_{0.07}O_2$	3.0179 (2)	17.0826 (7)	144.739 (5)
$CuCr_{0.90}Zn_{0.10}O_2$	3.1612 (5)	17.0819 (3)	146.163 (8)

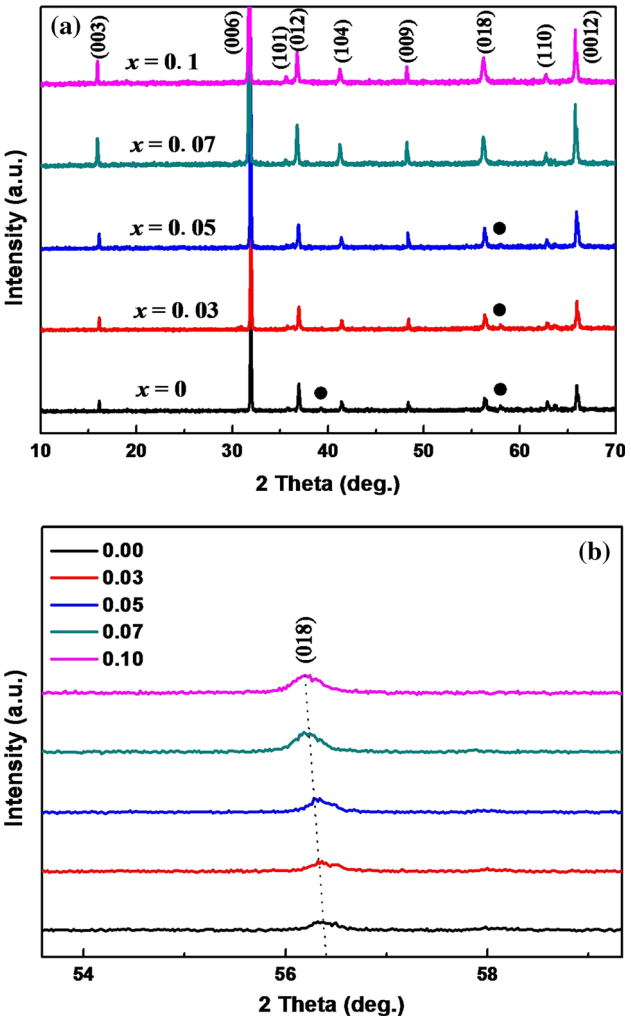

Fig. 2 a XRD patterns of the $CuCr_{1-x}Zn_xO_2$ ($x = 0$, 0.03, 0.05, 0.07, 0.1) samples, where *black circle* represents CuO. **b** Enlarged XRD pattern of $CuCr_{1-x}Zn_xO_2$ ($x = 0$, 0.03, 0.05, 0.07, 0.1) samples at (018) peak (Color figure online)

To further study the doping effect on the structure, Raman spectroscopy was measured for these samples. As shown in Fig. 3, the Raman spectrum of $CuCr_{1-x}Zn_xO_2$ ($x = 0$, 0.03, 0.05, 0.07, 0.1) shows three typical vibrational bands of delafossite structure. Similar results can be found in the earlier results for $CuGaO_2$ [21] and $CuCrO_2$ [22]. These bands are identified as $\sigma(A_{1g})$ at 691 cm^{-1}, $\sigma(E_g)$ at 444 cm^{-1} and $\sigma(A_g)$ at 207 cm^{-1}. It suggests that these vibrations may be associated with the spectral features of the edge-sharing $C^{III}O_6$ octahedra and possibly the O–Cu^{I}–O linear bond. The substitution of Cr by Zn induces abrupt changes in frequency and inline width of the A_{1g} and E_g modes. The shift of the two frequencies to shorter wave

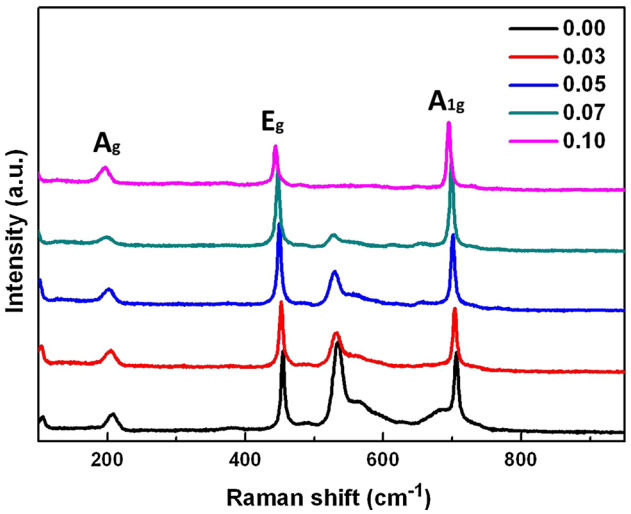

Fig. 3 Raman spectra of the $CuCr_{1-x}Zn_xO_2$ ($x = 0$, 0.03, 0.05, 0.07, 0.1) samples at room temperature (Color figure online)

numbers, indicating a weak (Cr, Zn)–O bonding, is consistent with the observed lattice expansion along different axes and with the difference in ionic radii between Cr^{3+} and Zn^{2+}. The A_{1g} mode, in particular, is shifted by up to 33 cm^{-1}, and the A_{1g} mode frequency is very sensitive to (Cr, Zn)-site atom-oxygen bonding characteristics.

For these Zn-doped samples, we also note a strong decrease in the intensity of the initially strong band around 535 cm^{-1}, and also the A_{1g}–E_g mode magnitude ratio is reverted. We suggest that the decrease in intensity is related to the decreased disorder. For the delafossite $CuCrO_2$ structure, the Cu cation is too small as compared with Cr cation, which results in tilt and twist of the CrO_6 octahedral. Then, the frame around the Cu cation collapses, and local symmetry may be severely damaged. Since Cu ion and Zn ion are with a similar size, the doping of Zn ions maintains the delafossite structure, and the disorder of CrO_6 octahedral is weakened. When the doping ratio reaches a certain value, local disorder disappears completely. Therefore, the doping of Zn ions in $CuCrO_2$ structure plays an important role in stabilizing the phase structure.

The above results confirm that the substitution of Cr by Zn in the investigated concentration range will possibly maintain the delafossite structure of the oxides. However, local changes do arise because of doping. These changes are much more obvious in Raman spectroscopy than in XRD due to good local probe property of the former characterization method.

XPS analysis

Figure 4 shows the Zn-2p and Cr-2p spectra of the $CuCr_{1-x}Zn_xO_2$ oxides. In the Zn-2p spectrum, two distinct peaks with two corresponding binding energies of $Zn–2p_{3/2} = 1021.4$ and $Zn–2p_{1/2} = 1044.5$ eV are observed, which indicates that the valence state of Zn ions is +2 through the comparison with the National Institute of Standards and Technology (NIST) X-ray photoelectron spectroscopy database. As shown in Fig. 4b, the two strong peaks in the Cr–2p spectrum at 576 and 585.7 eV for $2p_{3/2}$ and $2p_{1/2}$ peaks, respectively, indicate that the valence state of Cr ions is +3 [23]. Consequently, the oxidation state of Zn ions for the $CuCr_{1-x}Zn_xO_2$ samples stably exists in divalent state as Zn^{2+} oxidation.

Besides, in the Zn-doped $CuCrO_2$ system, the charge balance can be explained as below. Because of Zn-doping, the substitutional defect of "Zn_{Cr}" will be generated, which has a negative charge. At the same time, an oxygen atom vacancy defect of "Vo" will also be produced. Therefore, the overall charges are balanced in Zn-doped $CuCrO_2$.

FTIR analysis

FTIR absorption band in the range of 4000–400 cm^{-1} is usually assigned to the vibration of ions in crystal lattice. As shown in Fig. 5, the bonding vibration of $CuCr_{1-x}Zn_xO_2$ delafossite is within the range of 540–731 cm^{-1}. For the five samples, the apparition of the peaks centered at 540 cm^{-1} is assigned to the absorption of Cu–O stretching vibration [24]. The peak around 704 cm^{-1} presents the Cr–O stretching vibrations in CrO_6 distorted octahedral [25]. This is the energy of phonon vibration to cooperate with photon energy for electron transition in inter-band of allowed indirect gap. Besides, the peaks of the Cr–O stretching are 712, 718, 724, and 731 cm^{-1} for the $CuCr_{1-x}Zn_xO_2$ samples with $x = 0.03$, 0.05, 0.07, and 0.1,

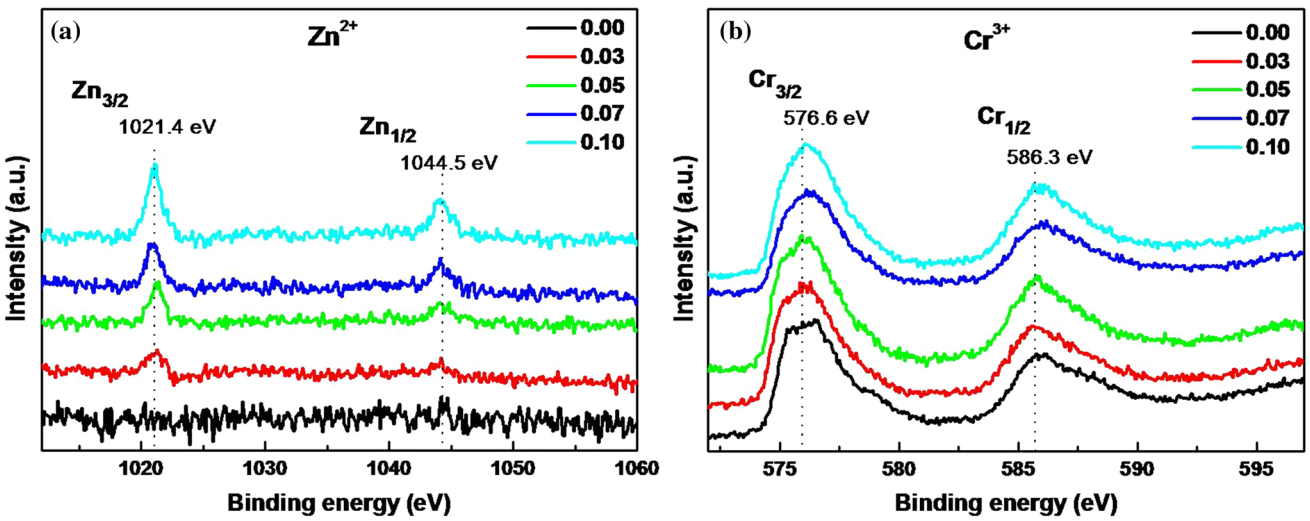

Fig. 4 XPS of **a** Cr-2p, **b** Zn–2p for the $CuCr_{1-x}Zn_xO_2$ samples ($x = 0$, 0.03, 0.05, 0.07, 0.1) (Color figure online)

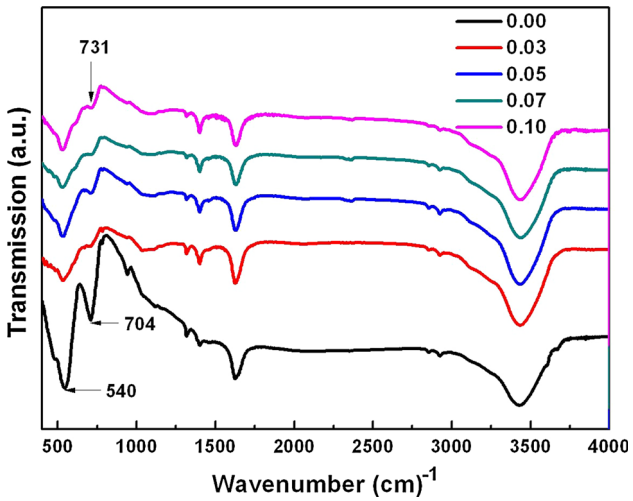

Fig. 5 FTIR spectra of $CuCr_{1-x}Zn_xO_2$ ($x = 0$, 0.03, 0.05, 0.07, 0.1) at room temperature (Color figure online)

respectively. The shift of the peak towards higher wavenumber is due to the Cr(Zn)–O stretching vibrations in weakened distorted octahedral as the substitution of Zn for Cr. In addition, the absorption of water stretching vibration peak around 3430 cm^{-1} can be observed. The intensity of the deformation vibration absorption peak near 1627 cm^{-1} slightly decreases with the increase of particle size. The reason is that, as the increase of the ratio between $CuCr_{1-x}Zn_xO_2$ particle size and its specific surface area, the absorbed water volume increases.

Thermal analysis

Thermal analysis was carried out to measure the process of the stable product formation. The $CuCrO_2$ powder was preheated at 300 °C in air in order to remove organic material, and thermo grams were recorded using a slowly heated sample with 10 °C/min from the ambient temperature to 1000 °C. Figure 6 shows the TG–DTA result of the $CuCrO_2$ sample. It can be seen that there is a 4 % weight gain at 430 °C, accompanied with an exothermic process. This abrupt increase and oxide exothermic peaks between 430 and 700 °C are probably due to the chemical reaction between Cu, Cr, and O to form $CuCr_2O_4$ and CuO. The final 4 % weight loss occurs around 850 °C, along with an endothermic process. This abrupt decrease is probably caused by the transformation of the phase $CuCr_2O_4$ to the delafossite phase as the following reaction

$$CuCr_2O_4 + CuO \rightarrow 2CuCrO_2 + 1/2O_2 \uparrow$$

The TG–DTA pattern indicates that the sintering temperature for obtaining stable phase should be higher than 850 °C.

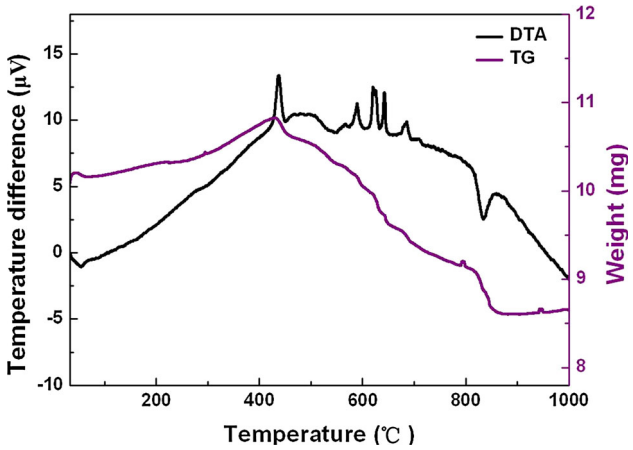

Fig. 6 TG–DTA pattern of the prepared $CuCrO_2$ sample (Color figure online)

Electrical properties analysis

A Hall measurement was carried out on the $CuCr_{1-x}Zn_xO_2$ ($x = 0$, 0.03, 0.05, 0.07, 0.1) pellets at room temperature for deciding carrier type and concentration. The results show that the Hall constant of the samples are given positive sign, indicating the carriers are holes and the samples are p-type conductors. The measured values of Hall constants (R_H) are 15.36, 11.41, 9.81, 7.12, 5.94 (m^3/C) for the samples with $x = 0$, 0.03, 0.05, 0.07, and 0.1, respectively. Then carrier concentration can be calculated from Hall constant by the formula $p = 1/e\ R_H$, where e is electron charge. The hole carrier concentrations are calculated to be 4.07×10^{17}, 5.48×10^{17}, 6.37×10^{17}, 8.78×10^{17}, 1.05×10^{18} cm^{-3} for the five samples. The results show that the hole concentration gets higher with the increase of Zn-doping ratio.

The Seebeck coefficient (S) and the temperature-dependent conductance were simultaneously measured on the 2.5 mm × 2.5 mm × 15 mm pellets for $CuCr_{1-x}Zn_xO_2$ ($x = 0$, 0.05, 0.1). As shown in Fig. 7a, the Seebeck coefficients of the $CuCr_{1-x}Zn_xO_2$ samples are positive over the measured range. This confirms that the samples are p-type conductors and the major conductive carriers are holes. The Seebeck coefficient increases as temperature gets higher, which probably results from some effects such as thermal expansion, grain boundary barrier effect or the change of bandwidth and gap energy. The relationship between the Seebeck coefficient and temperature is related by $S = (k_B/e)[(E_{as}/k_BT) + A]$, where k_B is Boltzmann's constant, E_{as} is the energy difference between the upper valence-edge energy (E_v) and the Fermi energy level (E_F), T is absolute temperature, and A is a constant [26]. The value of E_{as} is obtained by the linear plotting of S as a function of $1000/T$, which corresponds to the Fermi energy level in semiconductor. The results of E_{as} for $x = 0$, 0.05,

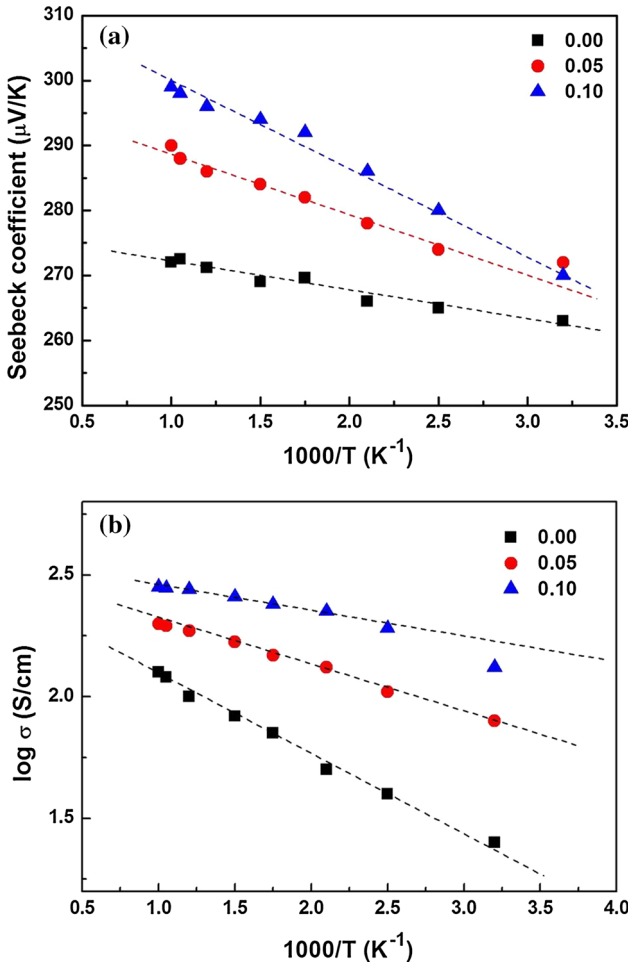

Fig. 7 Curves of **a** Seebeck coefficient and **b** logσ versus 1000/T for the $CuCr_{1-x}Zn_xO_2$ ($x = 0$, 0.05, 0.1) samples

0.1 are approximately 53, 71 and 80.5 meV, respectively, which reveals that as the Zn content increases, the Fermi energy level of $CuCr_{1-x}Zn_xO_2$ also increases.

For p-type $CuCrO_2$ conductor, electron transportation is controlled by the polaron hopping mechanism of hole carriers caused by the mixed valence Cu^+/Cu^{2+} on Cu–Cu layer [27]. The mixed valence Cu^+/Cu^{2+} results from the oxygen non-stoichiometry value (y) intercalating into $CuCrO_2$ structure, and thus $CuCrO_{2+y}$ is generated with a valence formula of $\left[Cu^+_{1-2y}Cu^{2+}_{2y}\right]Cr^{3+}O_{2+y}$. For p-type $CuCr_{1-x}Zn_xO_2$, the electrical conduction is affected by the substitution of Zn^{2+} for Cr^{3+}, producing the mixed copper valence [Cu^+/Cu^{2+}] as well as the valence formula of $\left[Cu^+_{1-2x}Cu^{2+}_{2x}\right]\left[Cr^{3+}_{1-x}Zn^{2+}_x\right]O_2$. Also, the polaron carriers can hop between Cu^+ and Cu^{2+} sites on Cu–Cu plane and between Zn^{2+} and Cr^{3+} sites in octahedral layer for electrical conduction.

The electrical conductivity for a semiconductor can be described by the equation of $\sigma = \sigma_0 \exp(-E_{a\sigma}/k_BT)$, where $E_{a\sigma}$ is the activation energy of conduction, T is the absolute temperature, and σ_0 is a constant [27]. For p-type $CuCr_{1-x}Zn_xO_2$ ($x = 0.03$, 0.05, 0.07, 0.1), the activation energy corresponds to the energy for polaron used to hop between Zn^{2+} and Cr^{3+} sites, which can be directly obtained by the slope of the curve of logσ versus 1000/T. The curves of logσ versus 1000/T for the $CuCr_{1-x}Zn_xO_2$ ($x = 0$, 0.05, 0.1) samples are shown in Fig. 7b. The negative slopes of the straight lines indicate positive value of activation energy of conduction. The obtained values of $E_{a\sigma}$ are 54, 41.5, and 32 meV for $CuCr_{1-x}Zn_xO_2$ with $x = 0$, 0.05, 0.1, respectively. Also, the value of $E_{a\sigma}$ is found to decrease with the increase of Zn-doping concentration. The decrease of activation energy indicates that the polarons have low energy for hopping and thus for easy conduction.

Therefore, compared with the activation energy for polaron hopping between Cu^+ sites and Cu^{2+} sites before Zn-doping, the energy between Zn^{2+} sites and Cr^{3+} sites after Zn-doping becomes lower. Also, the activation energy can be decreased by increasing the Zn-doping concentration. The observed decrease of activation energy suggests an increase of conductivity, which may be interpreted by oxygen vacancy migration as reported in other studies on delafossite materials [28–30]. Furthermore, due to the decrease of resistivity with the increase of temperature, we can draw the conclusion that the conductivity of the $CuCrO_2$ and $CuCr_{1-x}Zn_xO_2$ samples is thermally activated. A similar phenomenon can be found in the reported Ti-doped Fe_2O_3 by Shawn Chatman et al. [31]. Also, L. Farrell et al. found that the measured activation energy in Mg-doped Cr_2O_3 powder decreases even for low Mg-doping [32].

Conclusion

P-type delafossite $CuCr_{1-x}Zn_xO_2$ ($x = 0$, 0.03, 0.05, 0.07, 0.1) oxides have been synthesized by sol–gel method. XRD and Raman spectra reveal the delafossite structure of the samples, and XPS results confirm that the chemical valence states of Cr and Zn ions are +3 and +2, respectively. FTIR spectra show the absorption of Cu–O and Cr–O stretching vibration. Seebeck and Hall coefficient reveal p-type conductive characteristics of the samples. Moreover, with the increase of Zn content, Fermi energy level increases, while the activation energy decreases. Therefore, the $CuCr_{1-x}Zn_xO_2$ delafossite compound can be a good candidate for p-type transparent conductive oxide semiconductor materials.

Acknowledgements This work was supported in part by the National Natural Science Foundation of China (Nos. 11404129,

61307124), National Key Technology R&D Program (Nos. 2013BAK06B04, 2014BAD08B03), Science and Technology Department of Jilin Province (No. 20140307014SF), Changchun Municipal Science and Technology Bureau (Nos. 11GH01, 14KG022) and the State Key Laboratory of Integrated Optoelectronics, Jilin University (No. IOSKL2012ZZ12).

References

1. Ginley D, Roy B, Ode A, Warmsingh C, Yoshida Y, Parilla P, Teplin C, Kaydanova T, Miedaner A, Curtis C (2003) Non-vacuum and PLD growth of next generation TCO materials. Thin Solid Films 445:193–198
2. Harvey SP, Mason TO, Gassenbauer Y, Schafranek R, Klein A (2006) Surface versus bulk electronic/defect structures of transparent conducting oxides: I. Indium oxide and ITO. J Phys D: Appl Phys 39:3959
3. Popovich ND, Wong SS, Ufer S, Sakhrani V, Paine D (2003) Electron-transfer kinetics at ITO films: influence of oxygen plasma. J Electrochem Soc 150:H255–H259
4. Nomura K, Shibata N, Maeda M (2002) Preparation of zinc oxide thin films by pulsed current electrolysis. J Electrochem Soc 149:F76–F80
5. Park DH, Cho YH, Do YR, Ahn BT (2006) Characterization of Eu-doped SnO_2 thin films deposited by radio-frequency sputtering for a transparent conductive phosphor layer sensors and displays: principles, materials, and processing. J Electrochem Soc 153:H63–H67
6. Kawazoe H, Yasukawa M, Hyodo H, Kurita M, Yanagi H, Hosono H (1997) P-type electrical conduction in transparent thin films of $CuAlO_2$. Nature 389:939–942
7. Dong G, Zhang M, Lan W (2008) Structural and physical properties of Mg-doped $CuAlO_2$ thin films. Vacuum 82:1321–1324
8. Dong G, Zhang M, Zhaeo X, Hui Yana, Chunyu Tianb, Yonggang Renb (2010) Improving the electrical conductivity of $CuCrO_2$ thin film by N doping. Appl Surf Sci 256:4121–4124
9. Nakanishi A, Katayama-Yoshida H (2012) Computational materials design for superconductivity in hole-doped delafossite $CuAlO_2$: transparent superconductors. Solid State Commun 152:24–27
10. Dong G, Zhang M, Wang M, Tang F, Li H, Huang A, Yan H (2012) Synthesis, electrical and optical properties of $CuNdO_2$ compound. J Phys Chem Solids 73:1170–1172
11. Chuai YH, Hu B, Li YD, Shen HZ, Zheng CT, Wang YD (2015) Effect of Sn substitution on the structure, morphology and photoelectricity properties of high c-axis oriented $CuFe_{1-x}Sn_xO_2$ thin film. J Alloy Compd 627:299–306
12. Han MJ, Jiang K, Zhang JZ, Li YW, Hu ZG, Chu JH (2011) Temperature dependent phonon evolutions and optical properties of highly c-axis oriented $CuGaO_2$ semiconductor films grown by the sol-gel method. Appl Phys Lett 99:131104
13. Jlaiel F, Elkhouni T, Amami M, Strobel P, Ben Salah A (2013) Structural and physical properties of the (Ca, Mg)-doped delafossite powder $CuGaO_2$. Mater Res Bull 48:1020–1026
14. Han MJ, Duan ZH, Zhang JZ, Zhang S, Li YW, Hu ZG (2013) Electronic transition and electrical transport properties of delafossite $CuCr_{1-x}Mg_xO_2$ ($0 \leq x \leq 12\%$) films prepared by the sol-gel method: a composition dependence study. J Appl Phys 114:163526
15. Duan N, Sleight AW, Jayaraj MK, Tate J (2000) Transparent p-type conducting $CuScO_{2+x}$ films. Appl Phys Lett 77:1325
16. Shannon RD (1976) Revised effective ionic radii and systematic studies of interatomic distances in halides and chalcogenides. Acta Cryst A32:751–767
17. Jiang HF, Zhu XB, Lei HC, Li G, Yang ZR, Song WH, Dai JM, Sun YP, Fu YK (2011) Effects of Mg substitution on the structural, optical, and electrical properties of $CuAlO_2$ thin films. J Alloy Compd 509:1768–1773
18. Dong P, Zhang M, Dong GB, Zhao XP, Yan H (2008) The optical and electrical properties of Zn-doped $CuAlO_2$ thin films deposited by RF magnetron sputtering semiconductor devices, materials, and processing. J Electrochem Soc 155:H319–H322
19. Kakehi Y, Satoh K, Yoshimura T, Ashida A, Fujimura N (2010) Effects of Mg doping on structural, optical, and electrical properties of $CuScO_2$(0001) epitaxial films. Vaccum 84:618–621
20. Jayalakshmi V, Murugan R, Palanivel B (2005) Electronic and structural properties of $CuMO_2$ (M = Al, Ga, In). J Alloys Compd 388:19–22
21. Pellicer-Porres J, Segura A, Martinez E (2005) Erratum: vibrational properties of delafossite $CuGaO_2$ at ambient and high pressures. Phys Rev B 72:064301–064306
22. Jlaiel F, Amami M, Boudjada N, Strobel P, Ben Salah A (2011) Metal transition doping effect on the structural and physical properties of delafossite-type oxide $CuCrO_2$. J Alloys Compd 509:7784–7788
23. Chen HY, Chang KP, Yang CC (2013) Characterization of transparent conductive delafossite-$CuCr_{1-x}O_2$ films. Appl Surf Sci 273:324–329
24. Banerrjee AN, Kundoo S, Chattoopadhyay KK (2003) Synthesis and characterization of p-type transparent conducting $CuAlO_2$ thin film by DC sputtering. Thin Solid Films 440:5–10
25. Banerjee AN, Maity R, Chattopadhyay KK (2004) Preparation of p-type transparent conducting $CuAlO_2$ thin films by reactive DC sputtering. Mater Lett 58:10–13
26. Ko D, Urban JJ, Murray CB (2010) Carrier distribution and dynamics of nanocrystal solids doped with artificial atoms. J Nano Lett 10:1842–1847
27. Lalanne M, Barnabe A, Mathieu F, Tailhades Ph (2009) Synthesis and thermostructural studies of a $CuFe_{1-x}Cr_xO_2$ delafossite Solid Solution with $0 \leq x \leq 1$. Inorg Chem 48:6065–6071
28. Nozaki T, Hayashi T, Kajitani T (2007) Structural, magnetic and thermoelectric properties of delafossite-type oxide, $CuCr_{1-x}Mg_xO_2$ ($0 \leq x \leq 0.05$). J Chem Eng Jpn 40:1205–1209
29. Benko FA, Koffyberg FP (1987) Opto-electronic properties of p- and n-type delafossite, $CuFeO_2$. J Phys Chem Solids 48:431–434
30. Rogers DB, Shannon RD, Prewitt CT, Gillson JL (1971) Chemistry of noble metal oxides. III. Electrical transport properties and crystal chemistry of ABO_2 compounds with the delafossite structure. J Inorg Chem 10:723–727
31. Shawn Chatman, Pearce Carolyn I, Rosso Kevin M (2015) Charge transport at Ti-doped hematite (001)/aqueous interfaces. Chem Mater 27:1665–1673
32. Farrell L, Fleischer K, Caffrey D, Mullarkey D, Norton E, Shvets IV (2015) Conducting mechanism in the epitaxial p -type transparent conducting oxide Cr2O3:Mg. Phys Rev B 91:125202